Invited paper

The role of filter banks in sinusoidal frequency estimation ☆

Andre Tkacenko, P.P. Vaidyanathan*

Department of Electrical Engineering 116-81, California Institute of Technology, 136-93 Moore, Pasadena, CA 91125, USA

Abstract

The problem of estimating the frequencies of sinusoids buried in noise has been one of great interest to the signal processing community for many years, especially to those involved in the field of array processing. While many methods have been proposed to solve this problem, most involve processing in the fullband. In this paper, we investigate the effects of carrying out estimation in the subbands of an analysis bank of a multirate filter bank and show that there are some benefits to be reaped. In particular, we observe that with properly chosen analysis filters, the local signal-to-noise ratio (SNR) and line resolution in the subbands will exceed that in the fullband. Also, through the use of the spectral flatness measure, we show that if the input noise is colored, then the noise processes seen in the subbands will be more flat on average. This can be useful if the exact statistics of the input noise process are not known. Various examples are shown giving evidence to the fact that estimation in the subbands is superior to that in the fullband. © 2001 The Franklin Institute. Published by Elsevier Science Ltd. All rights reserved.

Keywords: Sinusoidal frequency estimation; Pseudospectra; Filter banks; Subband estimation; Spectral flatness measure

1. Introduction

A classical problem of statistical signal processing [1–3] is that of determining the frequencies of sinusoids buried in noise. Such a problem arises in array processing

[4–6], for example, when we wish to estimate the direction of arrival (DOA) of a narrowband electromagnetic signal incident on a uniform linear array. In this application, the radial angle of arrival plays the role of digital frequency. Another field in which this problem arises is in digital telephony [7] when we wish to estimate one of the number of possible Caller ID tones.

While many approaches have been proposed to solve this problem, most suffer from certain basic shortcomings. For example, most require a large SNR and perform poorly if the lines are too close to one another. In this paper, we investigate how filter banks can be used to overcome these shortcomings. For a uniform maximally decimated power complementary analysis bank, we will see that locally in the subbands, the SNR and the line resolution increase by a factor equal to the decimation ratio. Examples will then be shown to demonstrate the usefulness of our claims. Afterwards, we will show that if the input noise is colored, then the noise processes seen in the subbands will be more white on the average in a certain quantitative sense. This will be shown heuristically and also analytically in terms of the spectral flatness measure. In particular, we will prove that for the class of maximally decimated power complementary analysis banks, the *geometric mean of the flatness measures of the subband signals* will exceed the flatness of the fullband signal. This is a generalization of a result given in [8], in which only ideal filters were considered. Examples of this result will also be shown and it will be seen that in many practical scenarios, we can assume the noise to be approximately white in the subbands, even though this may not be the case in the fullband. This will be useful if the statistics of the input noise are not known, which perhaps is more often the case than not.

1.1. Notations

Throughout the paper, we will use the notations described in [9]. In particular, boldface lowercase and uppercase letters will be used to represent vectors and matrices, respectively. The superscripts $(^*), (^T), (^\dagger), (^+)$, and $(^{+(\mathscr{P})})$ will be used to represent, respectively, the conjugate, transpose, conjugate transpose, Moore-Penrose pseudoinverse [10], and rank $\mathscr{P}$ pseudoinverse [1] of a given matrix. We will use the notation $[G(e^{j\omega})]_{\downarrow M}$ to denote the Fourier transform of $g(Mn)$. Finally, we will say that a signal $f(n)$, or its Fourier transform $F(e^{j\omega})$, is Nyquist(M) if $f(Mn) = \delta(n)$ or equivalently $[F(e^{j\omega})]_{\downarrow M} = 1$.

1.2. Outline

In Section 2, we briefly review some of the more classical methods for sinusoidal frequency estimation, including the Pisarenko harmonic decomposition [11], the MUSIC algorithm [12], and the principal components linear prediction method [13]. In Section 3, we analyze the effect of carrying out frequency estimation in the subbands of a uniform filter bank with ideal analysis filters for the case of white noise. It is shown there that the local SNR and line resolution increase by a factor equal to the decimation ratio. To substantiate our results, in Section 4, examples are

given in which estimation in the subbands performs better than in the fullband. In Section 5, we discuss some of the consequences involved when we deal with finite data records and show that the advantages mentioned above do not come without a price. Since in practice we must estimate correlation functions using only a finite amount of data, the estimated subband correlation functions will be more erroneous than the fullband one. In Section 6, we examine the effects of colored noise and show there that the geometric mean of the spectral flatnesses in the subbands exceeds that of the fullband for a particular class of filter banks. Examples are shown supporting this theorem in Section 7. In addition, we then compare estimation in the subbands to that in the fullband when the statistics of the noise are not known and the noise is incorrectly assumed to be white. It is seen there that estimation in the subbands continues to be superior to that in the fullband. In Section 8, we conclude by mentioning some of the open problems still present.

2. Problem statement and previous work

Regarding the problem of estimating sinusoids buried in noise, we have the following discrete time signal model $x(n)$:

$$x(n) = \sum_{i=1}^{\mathscr{P}} A_i s_i(n) + \eta(n), \quad s_i(n) = e^{j\omega_i n}, \quad A_i = |A_i| e^{j\phi_i}. \tag{1}$$

Here, we have $\mathscr{P}$ sinusoidal signals $s_i(n)$, each scaled by an amount A_i, and buried in the complex noise process $\eta(n)$. The goal here is to determine the frequencies ω_i of the sinusoidal signals given N_s observations of one particular instance of the random process $x(n)$. The complex amplitudes A_i are assumed to have unknown but constant magnitudes $|A_i|$ and phase angles ϕ_i each uniformly distributed over the interval $[-\pi, \pi)$. For sake of stationarity, it is assumed that the phase angles are pairwise independent, i.e. ϕ_i and ϕ_j are independent for all $i \neq j$. The noise process $\eta(n)$ is assumed to be a zero mean wide sense stationary (WSS) random process uncorrelated with the sinusoidal signals. Ideally, to estimate the frequencies given only N_s observations, we would use the maximum likelihood estimate. However, it turns out that if $\mathscr{P} > 1$, this problem becomes computationally intractable [2] as it involves finding the location of the global maximum of a highly nonlinear function. If N_s is sufficiently large, then the frequencies can be estimated by looking at the peaks of the magnitude of the Fourier transform of the observed signal, even if the power of the noise is significant. This is due to the fact that the sinusoids will have a Dirac type distribution in the frequency domain, whereas the observed noise signal will most likely not have such strong support in these regions. However, if N_s is relatively small, then these peaks will be smeared out in the frequency domain on account of the noticable windowing effect in the time domain. Since the approximate frequency resolution will vary as $2\pi/N_s$, lines that are close to each other (in particular, closer than $2\pi/N_s$) will become indistinguishable and will be observed as only one wide peak. Instead what is typically done in this case is to exploit the special

properties of the autocorrelation function of $x(n)$. This can be done since under the above assumptions, $x(n)$ is ergodic in the mean and autocorrelation [2]. It follows that $x(n)$ is a zero mean WSS process with the following autocorrelation function.

$$R_{xx}(k) = \sum_{i=1}^{\mathscr{P}} P_i e^{j\omega_i k} + R_{\eta\eta}(k), \quad P_i \triangleq |A_i|^2. \tag{2}$$

Here, P_i denotes the power of the ith sinusoidal signal. At this point, we define two figures of merit for estimating the frequencies, namely the individual or local signal-to-noise ratio of the ith sinusoid with respect to the noise, denoted as $\mathrm{SNR}_{\mathrm{ind},i}$ and the net signal-to-noise ratio $\mathrm{SNR}_{\mathrm{net}}$. These are defined as follows.

$$\mathrm{SNR}_{\mathrm{ind},i} \triangleq \frac{P_i}{R_{\eta\eta}(0)}, \qquad \mathrm{SNR}_{\mathrm{net}} \triangleq \frac{\sum_{i=1}^{\mathscr{P}} P_i}{R_{\eta\eta}(0)}.$$

The local SNR is a good figure of merit of how likely we will be able to estimate a particular frequency correctly. As we would heuristically expect, it can be shown [2,5] that as this ratio increases for some sinusoid, indeed we will statistically estimate this sinusoid more correctly. The net SNR, on the other hand, is a measure of how likely we will be able to estimate the frequencies on average. Continuing from (2), the $N \times N$ autocorrelation matrix of $x(n)$, namely $\mathbf{R}_x$, is as follows:

$$\mathbf{R}_x = \sum_{i=1}^{\mathscr{P}} P_i \mathbf{s}_i \mathbf{s}_i^\dagger + \mathbf{R}_\eta = \mathbf{R}_s + \mathbf{R}_\eta, \quad \mathbf{s}_i \triangleq [1 \ e^{j\omega_i} \ \cdots \ e^{j(N-1)\omega_i}]^\mathrm{T}. \tag{3}$$

Here, the matrices $\mathbf{R}_s$ and $\mathbf{R}_\eta$ denote, respectively, the autocorrelation matrices corresponding to the purely harmonic process consisting of the $\mathscr{P}$ sinusoids and the noise process. As $\mathbf{R}_s$ is simply a sum of dyadic matrices of the form $\mathbf{v}\mathbf{v}^\dagger$, it can be shown [2] that if the frequencies ω_i are all distinct modulo 2π and if the size of the autocorrelation matrix N is chosen such that $N > \mathscr{P}$, then $\mathbf{R}_s$ has rank $\mathscr{P}$. Furthermore, the set of $\mathscr{P}$ eigenvectors $\{\mathbf{v}_k\}$ for $k = 1, ..., \mathscr{P}$ corresponding to the nonzero eigenvalues $\{\lambda_k\}$ span the same space as the signal vectors $\{\mathbf{s}_i\}$. The space spanned by the signal vectors $\{\mathbf{s}_i\}$ is commonly referred to as the *signal subspace*. The remaining $N - \mathscr{P}$ eigenvectors $\mathbf{v}_k$ for $k = \mathscr{P} + 1, ..., N$ corresponding to the zero eigenvalue are orthogonal to all of the signal vectors, i.e. $\mathbf{s}_i^\dagger \mathbf{v}_k = 0$ for all $i = 1, ..., \mathscr{P}$ and $k = \mathscr{P} + 1, ..., N$. The space spanned by the eigenvectors $\{\mathbf{v}_k\}$ for $k = \mathscr{P} + 1, ..., N$ is commonly called the *noise subspace*. Define the eigenfilter corresponding to $\mathbf{v}_k = [v_k(0) \ v_k(1) \ \cdots \ v_k(N-1)]^\mathrm{T}$ as

$$V_k(z) \triangleq \sum_{n=0}^{N-1} v_k(n) z^{-n}.$$

Then, for $k = \mathscr{P} + 1, ..., N$, it follows that $V_k(z)$ has zeros at $z = e^{j\omega_1}, ..., e^{j\omega_{\mathscr{P}}}$. If the input noise process $\eta(n)$ is white with variance σ_η^2, then $\mathbf{R}_\eta = \sigma_\eta^2 \mathbf{I}$, and so we have

$$\mathbf{R}_x = \mathbf{R}_s + \sigma_\eta^2 \mathbf{I}.$$

In this case, the eigenvectors of $\mathbf{R}_x$ are the same as those of $\mathbf{R}_s$, namely $\mathbf{v}_k$ for $k = 1, \ldots, N$. The corresponding eigenvalues μ_k are given below as follows:

$$\mu_k = \begin{cases} \lambda_k + \sigma_\eta^2, & k = 1, \ldots, \mathscr{P}, \\ \sigma_\eta^2, & k = \mathscr{P} + 1, \ldots, N. \end{cases}$$

As $\mathbf{R}_x$ can be estimated by observations of $x(n)$, the frequencies of the sinusoids can be estimated by finding the roots of the eigenfilters $V_k(z)$ for $k = \mathscr{P} + 1, \ldots, N$ ideally on (or in practice nearest) the unit circle. This is the basis behind many of the classical techniques for sinusoidal frequency estimation which we discuss briefly below, such as the Pisarenko harmonic decomposition [11], the MUSIC algorithm [12], and the principal components linear prediction (PCLP) method [13]. These algorithms only work if the input noise is white. In Section VI, we address what must be done if the noise is colored.

2.1. Pisarenko harmonic decomposition

In 1973, Pisarenko became the first person to observe and exploit the interesting eigenstructure of the autocorrelation matrix $\mathbf{R}_x$ for the purpose of frequency estimation. In his classic paper [11], he used an autocorrelation matrix of size $N = \mathscr{P} + 1$ and estimated the frequencies as the peaks of the following frequency estimation function commonly referred to now as the "pseudospectrum" [1–3] corresponding to the Pisarenko harmonic decomposition.

$$\hat{S}_{\text{PHD}}(e^{j\omega}) = \frac{1}{|V_{\mathscr{P}+1}(e^{j\omega})|^2} \quad \text{where} \quad V_{\mathscr{P}+1}(z) = \sum_{n=0}^{\mathscr{P}} v_{\mathscr{P}+1}(n) z^{-n}.$$

Ideally, all of the zeros of $V_{\mathscr{P}+1}(z)$ lie on the unit circle at angles corresponding to the frequencies of the sinusoids sent. Thus, the frequencies are estimated as the locations of the peaks of $\hat{S}_{\text{PHD}}(e^{j\omega})$ or the zeros of $V_{\mathscr{P}+1}(z)$. Though this method works in theory, in practice it unfortunately performs poorly, even at large SNRs [1–3]. The reason for this is that with finite data records, the variance of $\hat{S}_{\text{PHD}}(e^{j\omega})$ is quite large on account of the small size of the autocorrelation matrix used [2]. By using a larger size, as is the case with the MUSIC algorithm and the PCLP method, we obtain frequency estimators which come much closer to the Cramér–Rao bound than the Pisarenko harmonic decomposition.

2.2. MUSIC algorithm

The MUltiple SIgnal Classification or MUSIC algorithm introduced by Schmidt in 1979 [12] is a generalization of the Pisarenko harmonic decomposition, which experimentally has been shown to be a major improvement over that method. Here, the size of the autocorrelation matrix $\mathbf{R}_x$ is chosen to be $N > \mathscr{P} + 1$ and the pseudospectrum is obtained by reciprocating the sum of the magnitude squared

responses of the eigenfilters $V_k(z)$ for $k = \mathscr{P} + 1, \ldots, N$, as is shown below.

$$\hat{S}_{\text{MUSIC}}(e^{j\omega}) = \frac{1}{\sum_{k=\mathscr{P}+1}^{N} |V_k(e^{j\omega})|^2}.$$

As before, the frequencies of the sinusoids are estimated to be where the peaks of the function above occur. However, note now that $V_k(z)$ is a polynomial of degree $N - 1 > \mathscr{P}$ for all k. Thus, while each $V_k(z)$ for $k = \mathscr{P} + 1, \ldots, N$ will have $\mathscr{P}$ roots on the unit circle corresponding to the frequencies of the sinusoids sent, it will also have $N - \mathscr{P} - 1$ roots, deemed spurious roots, which can lie anywhere in the complex plane, including the unit circle. Though this may appear to be a dilemma, it is highly unlikely that the spurious zeros of all of the eigenfilters will coincide, and so adding the magnitude responses in the denominator of the pseudospectrum above has the effect of moving these spurious roots away from the unit circle [1,3]. This method has been shown to perform well provided that the SNR is moderately large [1–3] and is still used today on account of its low complexity. However, the PCLP method, which elegantly takes care of the issue of spurious roots, has been shown experimentally to perform better, as will soon be discussed.

2.3. Principal components linear prediction

In 1982, Tufts and Kumaresan introduced a novel approach to estimate the frequencies of the sinusoids buried in noise [12]. They started from the known premise that for the harmonic process consisting of just the $\mathscr{P}$ sinusoids, whose autocorrelation matrix is simply $\mathbf{R}_s$, a prediction error filter could be found such that the prediction error variance is identically zero [1], provided that the size of the autocorrelation matrix N was such that $N > \mathscr{P}$. That is, if $\mathbf{a} \triangleq [a(0)\ a(1)\ \cdots\ a(N-1)]^T$ represents the vector of prediction error filter coefficients, then the normal equations to determine an optimal prediction filter are as follows [1]:

$$\mathbf{R}_s \mathbf{a} = \mathbf{0}. \tag{4}$$

From this, we observe that the vector $\mathbf{a}$ is an eigenvector corresponding to the zero eigenvalue and hence is orthogonal to the signal subspace. It turns out that for $N > \mathscr{P} + 1$, there is not a unique solution to (4), and as a result, the eigenfilter corresponding to $\mathbf{a}$, namely $A(z)$, will have $\mathscr{P}$ of its roots on the unit circle corresponding to the frequencies of the sinusoids sent and $N - \mathscr{P} - 1$ spurious roots which may lie anywhere in the complex plane. This is similar to what was observed above for the eigenfilters $V_k(z)$ in the case of the MUSIC algorithm. It turns out, however [1], that this problem can be overcome if we take $\mathbf{a}$ to be monic, i.e. $a(0) = 1$, and minimize the l^2-norm of the vector $\mathbf{a}$ subject to the constraint (4). By minimizing this norm, the problem becomes akin to solving for an optimum prediction error filter by the autocorrelation method. As a result, all spurious roots will be guaranteed to lie strictly inside the unit circle. Partitioning $\mathbf{a}$ as $\mathbf{a} = [1\ \hat{\mathbf{a}}^T]^T$ and $\mathbf{R}_s$ as $\mathbf{R}_s = [\mathbf{r}_s\ \hat{\mathbf{R}}_s]$, we have from (4),

$$\hat{\mathbf{R}}_s \hat{\mathbf{a}} = -\mathbf{r}_s$$

and so the *unique* optimal choice of $\hat{\mathbf{a}}$ which minimizes the l^2-norm of $\hat{\mathbf{a}}$ and hence $\mathbf{a}$ is given by [1],

$$\hat{\mathbf{a}} = -\hat{\mathbf{R}}_s^+ \mathbf{r}_s \tag{5}$$

where $\hat{\mathbf{R}}_s^+$ is the Moore–Penrose pseudoinverse [10] of the matrix $\hat{\mathbf{R}}_s$. Tufts and Kumaresan noted [13] that by choosing $\hat{\mathbf{a}}$ as in (5), the spurious roots of $A(z)$ had a tendency to be uniformly distributed around a circle (with radius less than unity of course) concentric with the unit circle at angles away from those which corresponded to the frequencies of the sinusoids sent. While this approach elegantly handles the spurious roots of the eigenfilter $A(z)$, in practice, we will only have an estimate for the autocorrelation matrix of the observed process $\mathbf{R}_x$. A naive approach to this problem is to partition $\mathbf{R}_x$ as $\mathbf{R}_x = [\mathbf{r}_x \ \hat{\mathbf{R}}_x]$ and choose $\hat{\mathbf{a}}$ as $\hat{\mathbf{a}} = -\hat{\mathbf{R}}_x^+ \mathbf{r}_x$. However, Tufts and Kumaresan showed that the presence of the noise in $\mathbf{R}_x$ had a tendency to significantly perturb $\hat{\mathbf{a}}$ from its optimum value given in (5). Instead, they showed [13] that the following choice of $\hat{\mathbf{a}}$ had the effect of nullifying the perturbation due to the present noise:

$$\hat{\mathbf{a}} = -\hat{\mathbf{R}}_x^{+(\mathscr{P})} \mathbf{r}_x,$$

where $\hat{\mathbf{R}}_x^{+(\mathscr{P})}$ is the rank $\mathscr{P}$ pseudoinverse [1] of the matrix $\hat{\mathbf{R}}_x$ obtained by preserving only the $\mathscr{P}$ largest singular values of $\hat{\mathbf{R}}_x^+$ and zeroing out the rest. This choice of $\hat{\mathbf{a}}$ forms the foundation for the principal components linear prediction method or PCLP method for estimating the frequencies of the sinusoids. In particular, if $\hat{\mathbf{a}} = [\hat{a}(1) \ \hat{a}(2) \ \cdots \ \hat{a}(N-1)]^T$, the frequencies are estimated as the $\mathscr{P}$ roots of the prediction error filter,

$$A(z) = 1 + \sum_{n=1}^{N-1} \hat{a}(n)z^{-n}$$

on or nearest the unit circle. Graphically, the frequencies are estimated as the peaks of the pseudospectrum,

$$\hat{S}_{\text{PCLP}} = \frac{1}{|A(e^{j\omega})|^2}. \tag{6}$$

While this method is computationally more complex than the MUSIC algorithm, there is evidence to support its superiority. In [2], it is shown for the case of two sinusoids that the PCLP method comes much closer to the Cramér–Rao bound for frequency estimation than does the MUSIC algorithm. It is also mentioned there that the choice of $N \approx \frac{3}{4}N_s$ has been shown experimentally to give the lowest variance estimate. Furthermore, in [13,1], it is shown that the method of (6) is relatively insensitive to an overestimation of the number of sinusoids in the received signal. Namely, if the number of sinusoids buried in the noise is not known a priori and is estimated erroneously to be $\mathscr{P}_0 > \mathscr{P}$, then provided that the noise power is of a moderate level, there will be only $\mathscr{P}$ dominant peaks observed in the pseudospectrum of (6). It is this property which allows estimation in the subbands of a filter bank to be possible, as we will soon see, since the number of sinusoids present in any one subband will not be known a priori. As the PCLP method has been shown

experimentally to approach the Cramér–Rao bound for frequency estimation closer than other techniques [2], we have opted to use this method for estimation in the subbands. At this point, we will proceed to analyze what happens when the model signal given in (1) is input to a filter bank.

3. Analysis of subband frequency estimation

3.1. Introduction

Suppose that $x(n)$ as in (1) is input to the M-channel maximally decimated uniform analysis bank as shown in Fig. 1. Regardless of the choice of analysis filters, the subband signals $v_m(n)$ and $x_m(n)$ for $m = 0, \ldots, M - 1$ are given by the following expressions:

$$v_m(n) = \sum_{i=1}^{\mathcal{P}} A_i H_m(\mathrm{e}^{\mathrm{j}\omega_i})\mathrm{e}^{\mathrm{j}\omega_i n} + w_m(n)$$

$$x_m(n) = \sum_{i=1}^{\mathcal{P}} A_i H_m(\mathrm{e}^{\mathrm{j}\omega_i})\mathrm{e}^{\mathrm{j}M\omega_i n} + \eta_m(n) \tag{7}$$

where $w_m(n) = h_m(n) * \eta(n)$ and $\eta_m(n) = w_m(Mn)$. As we can see from (7), the mth subband signal $x_m(n)$ consists of sinusoids buried in the noise process $\eta_m(n)$. The autocorrelation sequence of each subband signal is given by,

$$R_{x_m x_m}(k) = \sum_{i=1}^{\mathcal{P}} P_i |H_m(\mathrm{e}^{\mathrm{j}\omega_i})|^2 \mathrm{e}^{\mathrm{j}M\omega_i k} + R_{\eta_m \eta_m}(k). \tag{8}$$

Suppose now that the input noise is white with variance σ_η^2 and that the magnitude squared response of each analysis filter satisfies the Nyquist(M) property, i.e. $[|H_m(\mathrm{e}^{\mathrm{j}\omega})|^2]_{\downarrow M} = 1$ for all $m = 0, \ldots, M - 1$. Then it can easily be shown that each of
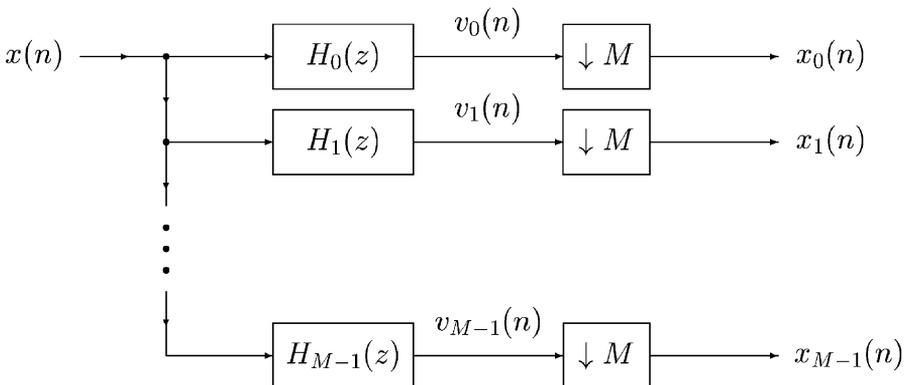

Fig. 1. The M-channel uniform analysis bank.

the noise processes $\eta_m(n)$ is white with variance σ_η^2. Thus, the mth subband signal $x_m(n)$ is nothing more than a set of sinusoids buried in the white noise process $\eta_m(n)$. It is clear here in this case that the subband signals $x_m(n)$ are intrinsically of the same form as the input signal $x(n)$. The only differences are that the sinusoids are scaled by the frequency responses of the analysis filters and the frequencies of the sinusoids themselves are mapped to different locations, namely $\omega_i \rightarrow M\omega_i \bmod 2\pi$. It will be seen shortly that these two very important differences make estimation in the subbands advantageous compared to that in the fullband.

3.2. Advantages of estimation in the subbands

3.2.1. SNR amplification

Suppose that the analysis filters are ideal and have a magnitude squared response as shown in Fig. 2. Clearly this choice of $|H_m(e^{j\omega})|^2$ satisfies $[|H_m(e^{j\omega})|^2]_{\downarrow M} = 1$ for all m as desired. In this case, we have

$$R_{x_m x_m}(k) = \sum_{\omega_i \in I_m} \underbrace{(MP_i)}_{\hat{P}_i} e^{jM\omega_i k} + \sigma_\eta^2 \delta(k).$$

Here, $\hat{P}_i = MP_i$ for $\omega_i \in I_m$ is the effective power of the sinusoids seen in the mth subband. From this, we conclude that the effective local SNR seen in the subbands is larger than that seen in the fullband by a factor of M, the decimation ratio. Quantitatively, we have, for $\omega_i \in I_m$,

$$\text{SNR}_{\text{ind},i,\text{sub}} = M(\text{SNR}_{\text{ind},i,\text{full}})$$

where $\text{SNR}_{\text{ind},i,\text{sub}}$ and $\text{SNR}_{\text{ind},i,\text{full}}$ are the local SNRs of the ith sinusoid in the mth subband and in the fullband, respectively. As there is an increase of the local SNR seen in the subbands, we expect to estimate the frequencies seen in the subbands more accurately than those seen in the fullband. As the intervals $\{I_m\}$ form a
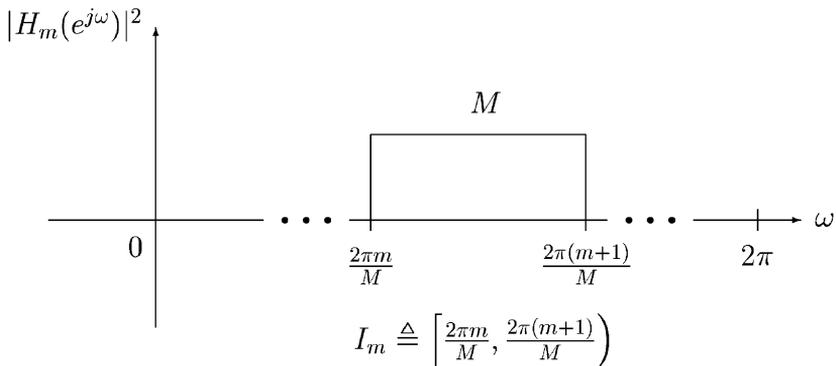

Fig. 2. Magnitude squared response of $H_m(z)$.

partition of $[0, 2\pi)$, each sinusoid present in the original signal will appear in one and only one subband.

3.2.2. Increase of line resolution

To see what happens to the effective spacing between frequencies observed in the subbands as compared to that in the fullband, consider the scenario depicted in Fig. 3. Here, ω_p and ω_q are chosen to lie in the interval I_m. In the fullband, the spacing between these two frequencies is simply $\Delta\omega_f = \omega_q - \omega_p$. Note that we can express ω_p and ω_q as follows:

$$\omega_p = \frac{2\pi m}{M} + \theta_p, \quad \omega_q = \frac{2\pi m}{M} + \theta_q, \quad \text{where } 0 \leqslant \theta_p, \ \theta_q < \frac{2\pi}{M}. \tag{9}$$

Hence, we obviously have $\Delta\omega_f = \theta_q - \theta_p$. As we can see from Fig. 4, the autocorrelation sequence of the mth subband is given as

$$R_{x_m x_m}(k) = MP_p e^{j\hat{\omega}_p k} + MP_q e^{j\hat{\omega}_q k} + \sigma_\eta^2 \delta(k),$$

where $\hat{\omega}_p$ and $\hat{\omega}_q$ are given by

$$\hat{\omega}_p = M\omega_p \bmod 2\pi, \quad \hat{\omega}_q = M\omega_q \bmod 2\pi.$$
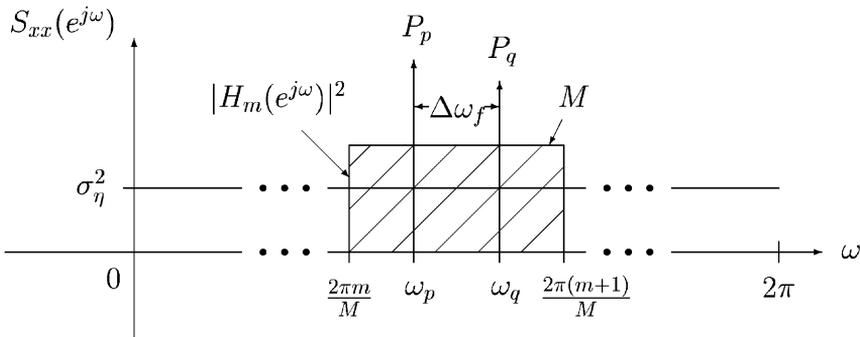

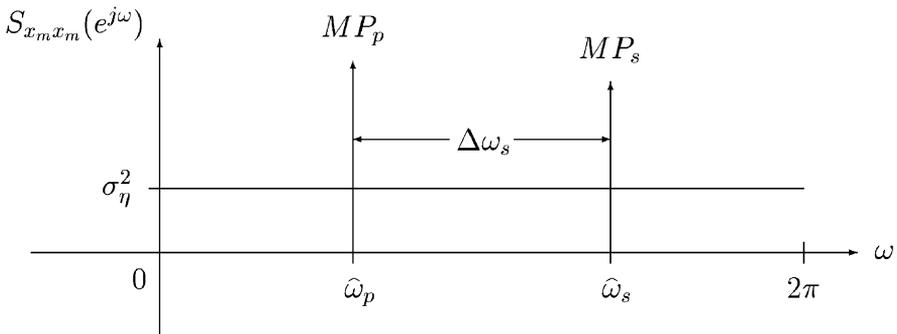Fig. 3. Input spectrum consisting of two closely spaced spectral lines.

Fig. 4. Subband spectrum consisting of two spectral lines.

From our expressions for ω_p and ω_q given in (9), it is clear that we have

$$\hat{\omega}_p = M\theta_p, \quad \hat{\omega}_q = M\theta_q.$$

Thus, the spacing between the frequencies present in the mth subband is simply $\Delta\omega_s = \hat{\omega}_q - \hat{\omega}_p = M(\theta_q - \theta_p)$. Clearly, we have

$$\Delta\omega_s = M\Delta\omega_f$$

and so the spacing between the frequencies in the mth subband is M times larger than it is in the fullband. As a result, the line resolution that we will have in the subbands will be greater than that in the fullband. This is important because traditional methods, such as the MUSIC algorithm and the PCLP method, have a certain frequency spacing threshold below which two closely spaced spectral lines will only be seen as one. For a detailed discussion of this principle, see [5]. In the next subsection, we discuss the important issue of mapping the frequencies seen in the subbands to those present in the fullband signal.

3.3. Mapping the subband frequencies to the fullband ones

From the results shown above, we expect that estimation in the subbands will be more accurate than that in the fullband. However, it should be kept in mind that the original problem is to determine the frequencies of the sinusoids of the fullband signal. As we will soon show, this mapping can be done in many circumstances, depending on the characteristics of the analysis filters used. To see this, note that from (8) we have

$$R_{x_m x_m}(k) = \sum_{i=1}^{\mathscr{P}} \hat{P}_{i,m} e^{j\hat{\omega}_{i,m}k} + R_{\eta_m \eta_m}(k),$$

where $\hat{P}_{i,m}$ and $\hat{\omega}_{i,m}$ are given by

$$\hat{P}_{i,m} = P_i |H_m(e^{j\omega_i})|^2, \quad \hat{\omega}_{i,m} = M\omega_i \bmod 2\pi \quad \forall i, m.$$

Note that the mapping between $\hat{\omega}_i$ and ω_i is not one-to-one. For example, if $\omega_1 = 2\pi/M$ and $\omega_2 = 4\pi/M$, then $\hat{\omega}_{1,m} = \hat{\omega}_{2,m} = 0$ for all m. Also note that the frequencies $\hat{\omega}_{i,m}$ are the same in each subband. Thus, the only degree of freedom we have in the mth subband is to vary the powers of the sinusoids seen there. It turns out that exploiting this degree of freedom will be all that will be needed to map the frequencies seen in the subbands correctly back to the fullband frequencies. First, we will discuss the mapping in the case of ideal analysis filters and then we will consider what happens when each analysis filter has overlap with its adjacent neighbors. In addition to considering this mapping for the complex signal model of (1), we will also consider the mapping for the real analog of this model, namely,
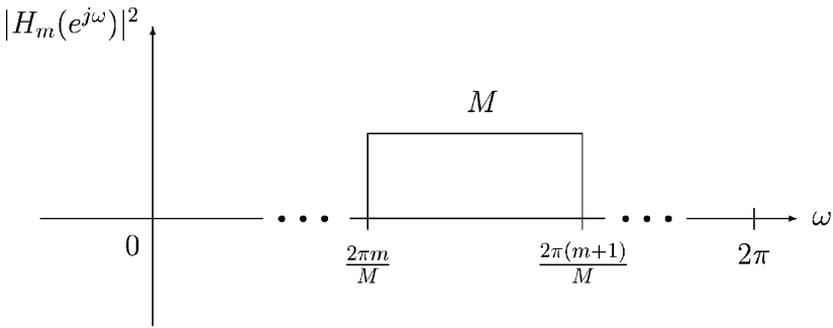
$$x(n) = \sum_{i=1}^{\mathscr{P}} C_i \cos(\omega_i n + \phi_i) + \eta_r(n). \tag{10}$$

Here, $\mathscr{P}$ denotes the number of real sinusoids present in $x(n)$, the amplitudes C_i are positive constants that are assumed to be unknown, the phases ϕ_i are identical in
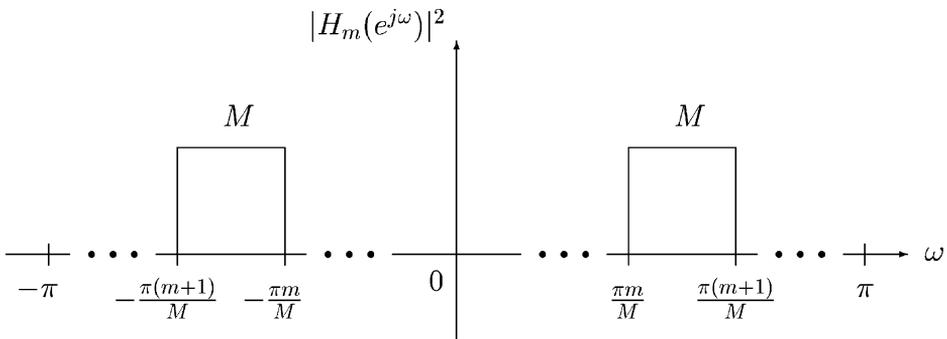
nature to those in (1), and the signal $\eta_r(n)$ is a real WSS noise process. As before, the goal is to determine the frequencies ω_i. However, since the signal $x(n)$ only consists of real sinusoids, the frequencies ω_i can now be assumed to be in the interval $[0, \pi]$ without loss of generality, instead of the interval $[0, 2\pi)$ in the case of the complex model given in (1). It turns out [2] that the model given in (10) satisfies very similar properties to the one considered in (1). In fact, the very same methods for frequency estimation considered in Section 2 can be applied here to obtain the frequencies ω_i. The advantages due to subband estimation mentioned above also hold true here for the model signal given in (10). However, since $x(n)$ in this case is real, it makes sense to consider real coefficient filters in which the magnitude response of each analysis filter is even.

3.3.1. Ideal filters

Suppose that the magnitude squared response of the mth analysis filter is given as in Fig. 5. Here, there is no spectral overlap between adjacent filters and so we can

(a)

(b)

Fig. 5. Ideal analysis filters for the model signal given in (1) and (10), respectively.

map subband frequencies to fullband ones simply by looking at each subband individually. In other words, we do not need to use the information from adjacent subbands to uniquely determine what frequencies were sent. Table 1 describes this mapping more quantitatively.

3.3.2. More realistic filters

In practice, we will not be able to have ideal filters, so we now consider more realistic filters in which there is overlap between adjacent filters as can be seen in Fig. 6. Because of the overlap, we will not be able to uniquely determine the fullband frequencies by what is seen in any one subband. In this case, an observed subband frequency $\omega_{i,m}$ will also be seen in a previous subband as $\omega_{p,m-1}$, or in a subsequent subband as $\omega_{q,m+1}$, depending upon the value of $\omega_{i,m}$. For example, for the complex model signal of (1), if $0 \leqslant \omega_{i,m} < \pi$, then this frequency will also be seen in the $(m-1)$th subband as $\omega_{p,m-1}$ for some p. In general, for the complex model of (1), if $0 \leqslant \omega_{i,m} < \pi$, then we have $\omega_{i,m} = \omega_{p,m-1}$ for some p and if $\pi \leqslant \omega_{i,m} < 2\pi$, then we have $\omega_{i,m} = \omega_{q,m+1}$ for some q. The case of the real model is slightly more complicated in the sense that the mapping depends on the parity of the subband in which the line is present. If $0 \leqslant \omega_{i,m} < \pi/2$, then we have $\omega_{i,m} = \omega_{p,m-1}$ for some p if m is even and $\omega_{i,m} = \omega_{q,m+1}$ for some q if m is odd. On the other hand, if $\pi/2 \leqslant \omega_{i,m} < \pi$, then we have $\omega_{i,m} = \omega_{q,m+1}$ for some q if m is even and $\omega_{i,m} = \omega_{p,m-1}$ for some p if m is odd. As pseudospectra peaks are roughly proportional to the amplitudes of the sinusoids present [5], most likely, the subband with the larger pseudospectra will be the one from which the original fullband line originated. If $S_m(e^{j\omega})$ denotes the pseudospectrum of the mth subband, then the frequencies in the subbands are mapped to the fullband as shown in Table 2.

4. Examples of subband estimation

We will consider estimating the frequencies of the sinusoids of the following real signal $x(n)$:

$$x(n) = C_1 \cos(\omega_1 n + \phi_1) + C_2 \cos(\omega_2 n + \phi_2) + \eta_r(n), \tag{11}$$

where we have the following:

$$C_1 = C_2 = \sqrt{2}, \quad \omega_1 = 0.57\pi, \quad \omega_2 = 0.58\pi, \quad \sigma_{\eta_r}^2 = 4, \quad N_s = 128.$$
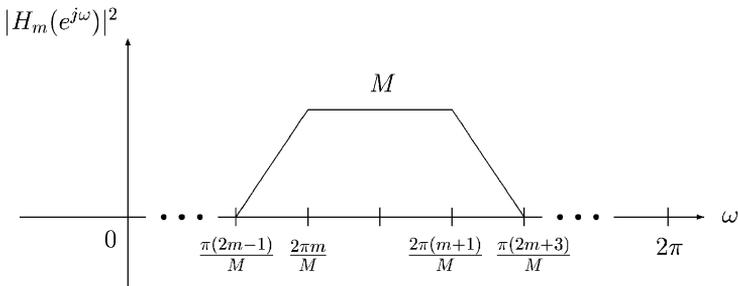
In this case, we have,

$$\text{SNR}_{\text{ind},1} = \text{SNR}_{\text{ind},2} = -6.02 \text{ (dB)}, \quad \text{SNR}_{\text{net}} = -3.01 \text{ (dB)}.$$
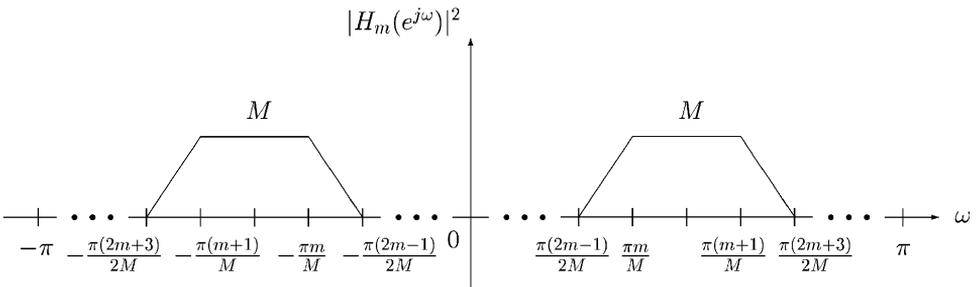
It should be noted here that as there are only $N_s = 128$ observations of $x(n)$ and the two frequencies are spaced out by $0.01\pi < 2\pi/128$, we cannot find the frequencies by taking the Fourier transform of the observed signal. As the input signal $x(n)$ is real

Table 1
Mapping the subband frequencies $\hat{\omega}_{i,m}$ to the fullband ones ω_l for the case of ideal filters as in Fig. 5

Model type	Fullband frequency: ω_l
Complex—Eq. (1)	$\dfrac{2\pi m + \hat{\omega}_{i,m}}{M}$
Real—Eq. (10)	$\begin{cases} \dfrac{\pi m + \hat{\omega}_{i,m}}{M}, & m \text{ even} \\[2mm] \dfrac{\pi(m+1) - \hat{\omega}_{i,m}}{M}, & m \text{ odd} \end{cases}$

(a)

(b)

Fig. 6. More realistic analysis filters for the model signal given in (1) and (10), respectively.

like the model given in (10), we will consider only cosine modulated analysis filter banks. In order to keep the number of observed samples seen in the subbands relatively moderate (see Section 5), the value of M is chosen to be 8. In the examples that follow, the estimation was carried out 50 times using a different observation of $x(n)$ each time.

Table 2
Mapping the subband frequencies $\hat\omega_{i,m}$ to the fullband ones ω_l for the case of nonideal filters as in Fig. 6

Model type	Fullband frequency: ω_l
Complex—Eq. (1)	$\dfrac{2\pi m - \hat\omega_{p,m-1}}{M}$, $\quad 0 \le \hat\omega_{i,m} < \pi,\ S_m(e^{j\hat\omega_{i,m}}) \le S_{m-1}(e^{j\hat\omega_{p,m-1}})$
	$\dfrac{2\pi m + \hat\omega_{i,m}}{M}$, $\quad 0 \le \hat\omega_{i,m} < \pi,\ S_m(e^{j\hat\omega_{i,m}}) \ge S_{m-1}(e^{j\hat\omega_{p,m-1}})$
	$\dfrac{2\pi m + \hat\omega_{i,m}}{M}$, $\quad \pi \le \hat\omega_{i,m} < 2\pi,\ S_m(e^{j\hat\omega_{i,m}}) \ge S_{m+1}(e^{j\hat\omega_{q,m+1}})$
	$\dfrac{2\pi(m+2) - \hat\omega_{q,m+1}}{M}$, $\quad \pi \le \hat\omega_{i,m} < 2\pi,\ S_m(e^{j\hat\omega_{i,m}}) \le S_{m+1}(e^{j\hat\omega_{q,m+1}})$
Real—Eq. (10)	m even $\Rightarrow$
	$\quad \dfrac{\pi m - \hat\omega_{p,m-1}}{M}$, $\quad 0 \le \hat\omega_{i,m} < \dfrac{\pi}{2},\ S_m(e^{j\hat\omega_{i,m}}) \le S_{m-1}(e^{j\hat\omega_{p,m-1}})$
	$\quad \dfrac{\pi m + \hat\omega_{i,m}}{M}$, $\quad 0 \le \hat\omega_{i,m} < \dfrac{\pi}{2},\ S_m(e^{j\hat\omega_{i,m}}) \ge S_{m-1}(e^{j\hat\omega_{p,m-1}})$
	$\quad \dfrac{\pi m + \hat\omega_{i,m}}{M}$, $\quad \dfrac{\pi}{2} \le \hat\omega_{i,m} < \pi,\ S_m(e^{j\hat\omega_{i,m}}) \ge S_{m+1}(e^{j\hat\omega_{q,m+1}})$
	$\quad \dfrac{\pi(m+2) - \hat\omega_{q,m+1}}{M}$, $\quad \dfrac{\pi}{2} \le \hat\omega_{i,m} < \pi,\ S_m(e^{j\hat\omega_{i,m}}) \le S_{m+1}(e^{j\hat\omega_{q,m+1}})$
	m odd $\Rightarrow$
	$\quad \dfrac{\pi(m+1) + \hat\omega_{q,m+1}}{M}$, $\quad 0 \le \hat\omega_{i,m} < \dfrac{\pi}{2},\ S_m(e^{j\hat\omega_{i,m}}) \le S_{m+1}(e^{j\hat\omega_{q,m+1}})$
	$\quad \dfrac{\pi(m+1) - \hat\omega_{i,m}}{M}$, $\quad 0 \le \hat\omega_{i,m} < \dfrac{\pi}{2},\ S_m(e^{j\hat\omega_{i,m}}) \ge S_{m+1}(e^{j\hat\omega_{q,m+1}})$
	$\quad \dfrac{\pi(m+1) - \hat\omega_{i,m}}{M}$, $\quad \dfrac{\pi}{2} \le \hat\omega_{i,m} < \pi,\ S_m(e^{j\hat\omega_{i,m}}) \ge S_{m-1}(e^{j\hat\omega_{p,m-1}})$
	$\quad \dfrac{\pi(m-1) + \hat\omega_{p,m-1}}{M}$, $\quad \dfrac{\pi}{2} \le \hat\omega_{i,m} < \pi,\ S_m(e^{j\hat\omega_{i,m}}) \le S_{m-1}(e^{j\hat\omega_{p,m-1}})$

Example 1. Kaiser–Window based prototype cosine modulated filter bank. In this example, the impulse responses of the analysis filters are given by [9],

$$h_k(n) = 2p_0(n) \cos\left[\frac{\pi}{M}\left(k + \frac{1}{2}\right)\left(n - \frac{N_p}{2}\right) + (-1)^k \frac{\pi}{4}\right] \tag{12}$$

for all k, n. Here, the sequence $p_0(n)$ is an FIR prototype filter of length N_p so that $h_k(n)$ has length N_p as well. The choice of $p_0(n)$ dictates the type of filter bank that we have. In this case, $p_0(n)$ was designed using the Kaiser–Window method as described in [14]. The length of each analysis filter here is $N_p = 40$. Fig. 7 shows the magnitude responses of the analysis filters. As we can see, the frequencies of the sinusoids present in (11) fall predominantly in the 3rd, 4th, and 5th subbands. The pseudospectra obtained here for the fullband, as well as the 3rd, 4th, and 5th subbands are shown in Fig. 8. As we can see, the pseudospectra seen in the fullband
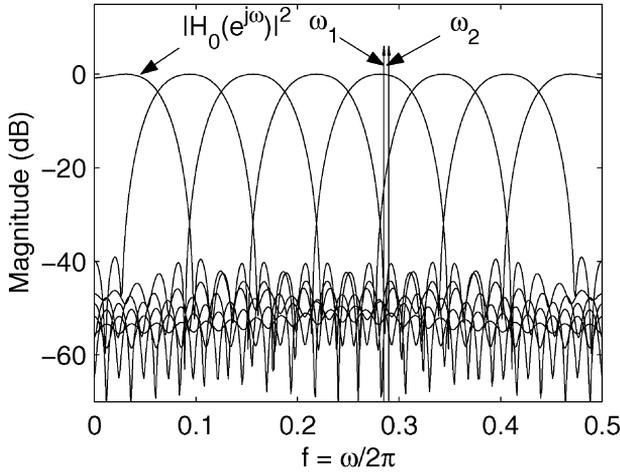
Fig. 7. Magnitude responses of the analysis filters designed using the Kaiser–Window method.
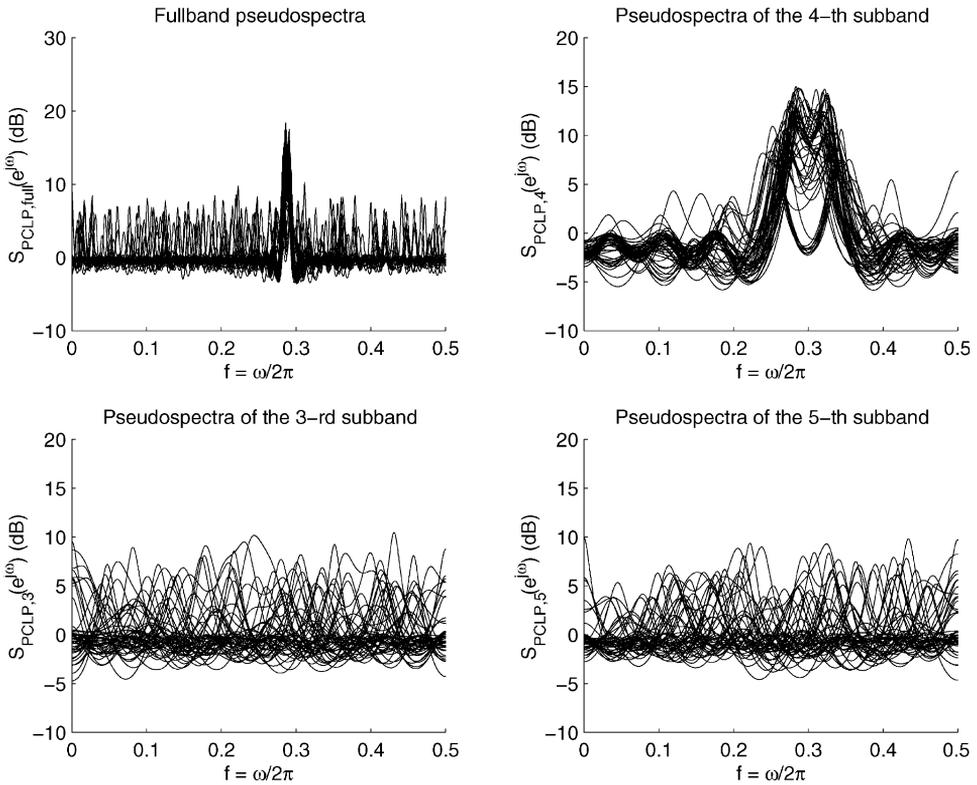

Fig. 8. Pseudospectra obtained for Example 1 (Kaiser CMFB).

only appear to consist of one predominant peak and we are not able to resolve both sinusoids. However, in the subband pseudospectra, we can clearly see the presence of two distinct lines. As the analysis filters provide good attenuation in the stopband, there is little overlap between adjacent filters and so the lines present in the 4th subband are heavily attenuated in the adjacent 3rd and 5th subbands, as is desired here. Performing the frequency mapping described in the previous section, we obtain the mean and standard deviation of the estimates of ω_1 and ω_2 shown in Table 3. Included in Table 3 are the results obtained by carrying out the estimation in the fullband. Here, we see that estimation in the subbands yielded better results.

Example 2. DCT IV filter bank. For this example, the analysis polyphase matrix [9] is simply the DCT IV matrix [15] and the impulse responses of the analysis filters are

$$h_k(n) = \sqrt{\frac{2}{M}} \cos\left[\frac{\pi}{M}\left(k + \frac{1}{2}\right)\left(n + \frac{1}{2}\right)\right]$$

for $k, n = 0, \ldots, M - 1$. Here, there is a significant amount of spillage between adjacent filters which will both hinder the performance and also make the mapping of frequencies more difficult as aliasing will be more predominant here. Because of this, the lines appear rather strongly in the 3rd, 4th, and 5th subbands. This phenomenon is not desired in practice, since it introduces ambiguity in the frequency mapping. Using the frequencies estimated in the 4th subband, where the lines are most predominant, we obtain the results shown in Table 3.

The results here are somewhat worse than what was obtained using the analysis filters of Example 1. This worse performance, on the other hand, is offset by the fact that this filter bank is much less computationally complex to implement than the one of Example 1. These examples serve to show that subband estimation methods can be used in cases where fullband methods will fail. In what follows, we consider some of the practical problems that result from subband estimation.

5. Consequences of subband estimation

We should note that the benefits due to subband estimation mentioned above do not come without a price. It is tempting to think that as the SNR and frequency resolution increase by a factor of M, the decimation ratio, we can achieve better and better estimation by taking M arbitrarily large. This, however, is certainly not the case in practice. The reason for this is that in practice autocorrelations have to be

Table 3
Comparison of fullband and subband methods for the case of white input noise

Method	$\bar{\omega}_1$ ($\omega_1 = 0.57\pi$)	$\bar{\omega}_2$ ($\omega_2 = 0.58\pi$)	$\sigma_{\bar{\omega}_1}$	$\sigma_{\bar{\omega}_2}$
Fullband	0.4892π	0.6262π	0.278182	0.110857
Kaiser CMFB	0.5678π	0.5817π	0.000286	0.000168
DCT	0.5664π	0.5883π	0.000506	0.001794

estimated from measured data. The quality of such an estimation is very heavily dependent upon the number of observations N_s of $x(n)$ available [5]. If, for example, the length of each analysis filter is N_f, then the length of each subband signal will be

$$\left\lfloor \frac{N_s + N_f - 2}{M} \right\rfloor + 1.$$

This number will typically be less than N_s. For Examples 1 and 2 above, the length of each subband signal was 21 and 17, respectively, whereas N_s was 128. To increase the length of the subband signals, a naive approach would be to increase the filter length and hence the complexity of the filter bank. While this can actually make the subband signals longer than the fullband observation of $x(n)$, such a large filter length will most likely introduce a bias in the estimate of the autocorrelation function of the subband signals. In such a case, there will be a windowing effect seen in the subbands on account of the small length signal observation $x(n)$ being filtered by the large length analysis filters. If all filter lengths are held fixed and M is increased, then the length of the subband signal will decrease.

As we can see, there is a tradeoff between the decimation ratio M and the length of each subband signal. It is because of this tradeoff that the value of M in Examples 1 and 2 was chosen conservatively to be 8. In practice, M should be carefully chosen to be large enough in order to reap the benefits of a large value of M, but small enough so that there are enough available samples in each subband. We will now focus on what happens when the input noise is not white and will find there that there is yet another advantage to doing estimation in the subbands.

6. The case of colored noise

6.1. Estimation in the fullband

Suppose that the given signal $x(n)$ is as in (1), where this time the noise process $\eta(n)$ is not white. Then the $N \times N$ autocorrelation matrix is given by (3) to be,

$$\mathbf{R}_x = \mathbf{R}_s + \sigma_\eta^2 \hat{\mathbf{R}}_\eta$$

where σ_η^2 is the variance of the noise process, i.e. $R_{\eta\eta}(0)$, and $\hat{\mathbf{R}}_\eta$ is a normalized autocorrelation matrix whose diagonal elements are all unity. With the case of white noise, we were able to determine the frequencies because $\mathbf{R}_x$ and $\mathbf{R}_s$ shared the same eigenvectors. For the case of colored noise, we linearly transform the vector of observations $\mathbf{x} \triangleq [x(0)\ x(1)\ \cdots\ x(N-1)]^T$ by the Karhunen–Loève transform or KLT of the normalized noise observation vector $\hat{\boldsymbol{\eta}} \triangleq 1/\sigma_\eta [\eta(n_0)\ \eta(n_0 + 1)\ \cdots\ \eta(n_0 + N - 1)]^T$. In practice, this requires first estimating $\hat{\mathbf{R}}_\eta$. The KLT is given by [11] as the following:

$$\mathbf{y} \triangleq \hat{\mathbf{R}}_\eta^{-1/2} \mathbf{x}.$$

This transformation diagonalizes $\hat{\mathbf{R}}_\eta$. We have,

$$\mathbf{R}_y = E[\mathbf{yy}^\dagger] = E[\hat{\mathbf{R}}_\eta^{-1/2}\mathbf{xx}^\dagger\hat{\mathbf{R}}_\eta^{-1/2}] = \hat{\mathbf{R}}_\eta^{-1/2}\mathbf{R}_x\hat{\mathbf{R}}_\eta^{-1/2},$$

where we have exploited the fact that $\hat{\mathbf{R}}_\eta^{-1/2}$ is Hermitian. As $\mathbf{R}_x$ can be estimated from the data, then we can form an estimate of $\mathbf{R}_y$ provided that we know the coloring of the noise process as manifested in the matrix $\hat{\mathbf{R}}_\eta$. To determine the frequencies of the original sinusoids, note that from (3) we have,

$$\mathbf{R}_y = \underbrace{\sum_{i=1}^{\mathscr{P}} P_i\mathbf{t}_i\mathbf{t}_i^\dagger}_{\mathbf{R}_t} + \sigma_\eta^2\mathbf{I}, \tag{13}$$

where the vectors $\mathbf{t}_i$ are defined to be,

$$\mathbf{t}_i \triangleq \hat{\mathbf{R}}_\eta^{-1/2}\mathbf{s}_i \tag{14}$$

As the vectors $\mathbf{s}_i$ are assumed to be linearly independent, assuming that the frequencies present in the input signal $x(n)$ are all distinct modulo 2π [2], the vectors $\mathbf{t}_i$ are all linearly independent. Thus, provided that $N > \mathscr{P}$, the matrix $\mathbf{R}_t$ in (13) is of rank $\mathscr{P}$ and furthermore the $\mathscr{P}$ eigenvectors $\{\mathbf{u}_k\}$ for $k = 1, \ldots, \mathscr{P}$ which correspond to the nonzero eigenvalues of $\mathbf{R}_t$ span the same subspace as the set of vectors $\{\mathbf{t}_i\}$. This was the same phenomenon observed in $\mathbf{R}_s$ in Section 2. Also, the eigenvectors of $\mathbf{R}_t$ which correspond to the zero eigenvalue, $\{\mathbf{u}_k\}$ for $k = \mathscr{P}+1, \ldots, N$, are orthogonal to the vectors $\mathbf{t}_i$, namely $\mathbf{t}_i^\dagger\mathbf{u}_k = 0$ for all $i = 1, \ldots, \mathscr{P}$ and $k = \mathscr{P}+1, \ldots, N$. Using (14), this means that $\mathbf{s}_i^\dagger(\hat{\mathbf{R}}_\eta^{-1/2}\mathbf{u}_k) = 0$ or that the generalized eigenfilter corresponding to $\hat{\mathbf{R}}_\eta^{-1/2}\mathbf{u}_k = [w_k(0)\ \ w_k(1)\ \ \cdots\ \ w_k(N-1)]^\mathrm{T}$, namely,

$$W_k(z) \triangleq \sum_{n=0}^{N-1} w_k(n)z^{-n}$$

has a zero at $z = e^{j\omega_i}$ for all $i = 1, \ldots, \mathscr{P}$ and $k = \mathscr{P}+1, \ldots, N$. From this property, we can obtain the original frequencies using either the MUSIC algorithm or PCLP method.

It should be noted that we can estimate the frequencies only if we know the noise autocorrelation matrix $\hat{\mathbf{R}}_\eta$. In practice, however, we may not know the exact statistics of the input noise. Despite this stumbling block, we will soon show that if the signal $x(n)$ is input to a particular kind of analysis bank, then, on average, the noise processes seen in the subbands will be more white in terms of the spectral flatness measure. There will even be some instances in which the flatness in each subband is strictly larger than that seen in the fullband. Hence, if we do not know the exact statistics of the noise process $\eta(n)$, then assuming that the noise is white in the subbands will be less erroneous than assuming that it is in the fullband. This will be illustrated with examples.
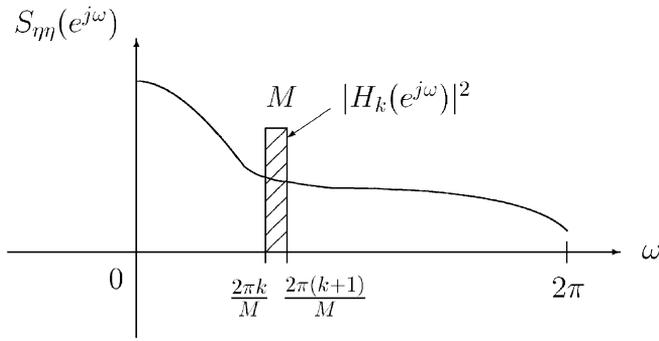
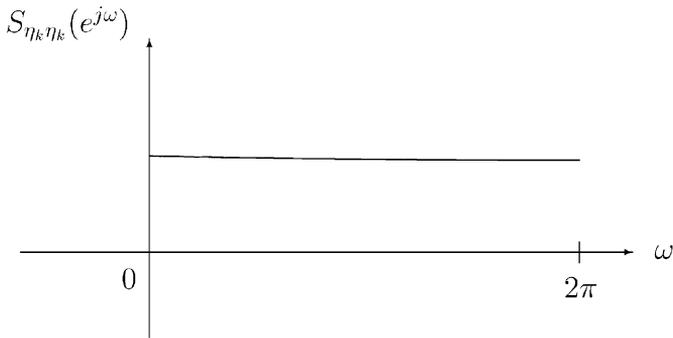Fig. 9. Example of a colored input noise power spectrum.

Fig. 10. The noise power spectrum of the kth subband.

6.2. Motivation for subband estimation

Suppose that the noise process $\eta(n)$ present in $x(n)$ as in (1) has a nonconstant power spectral density (psd) $S_{\eta\eta}(e^{j\omega})$ as shown in Fig. 9. Furthermore, suppose that the magnitude squared response of the mth analysis filter is given as in Fig. 2. An example for when $m = k$ is shown in Fig. 9. Then the psd of the noise process of the kth subband, namely $S_{\eta_k \eta_k}(e^{j\omega})$, is given as shown in Fig. 10. As we can see, the noise spectrum of the kth subband looks approximately constant whereas that of the fullband is certainly not. Heuristically, we can see that if the input noise statistics are not known, then we should expect less errors in assuming that the subband noise processes are white as opposed to assuming that the fullband process is white. If we take the decimation ratio M to be larger and larger, the noise processes in the subbands will look more and more white, regardless of the input noise spectrum. It should be remembered from Section 5 that in practice, we will not be able to take M arbitrarily large. Furthermore, ideal filters are unrealizable, and so we will only be able to use causal filters. However, this example serves to show that the noise processes seen in the subbands may be significantly more white than those seen in the

fullband. We will soon show quantitatively with the spectral flatness measure that indeed on average this is true.

6.3. The whitening of noise in the subbands

6.3.1. The spectral flatness measure

The *spectral flatness measure* γ_x^2 of a WSS random process $x(n)$ with psd $S_{xx}(e^{j\omega})$ is defined as follows [16]:

$$\gamma_x^2 \triangleq \frac{e^{\psi_x}}{\sigma_x^2} \quad \text{where } \psi_x = \frac{1}{2\pi} \int_{-\pi}^{\pi} \ln(S_{xx}(e^{j\omega})) \, d\omega. \tag{15}$$

This measure of flatness has the property that $0 \leqslant \gamma_x^2 \leqslant 1$, where $\gamma_x^2 = 1$ if $x(n)$ is white. For the purpose of estimating the frequencies of the sinusoids, we would like to have this measure as large as possible in the subbands, as we would like the noise seen in the subbands to be as white as possible.

6.3.2. Analysis of the flatness measures in the subbands

Suppose that any WSS random process $x(n)$ is input to the nonuniform M-channel analysis bank shown in Fig. 11. We will assume that this filter bank is maximally decimated, i.e. we have

$$\sum_{i=0}^{M-1} \frac{1}{n_i} = 1. \tag{16}$$

In addition, we will assume that the magnitude squared response of the ith filter is Nyquist(n_i), namely,

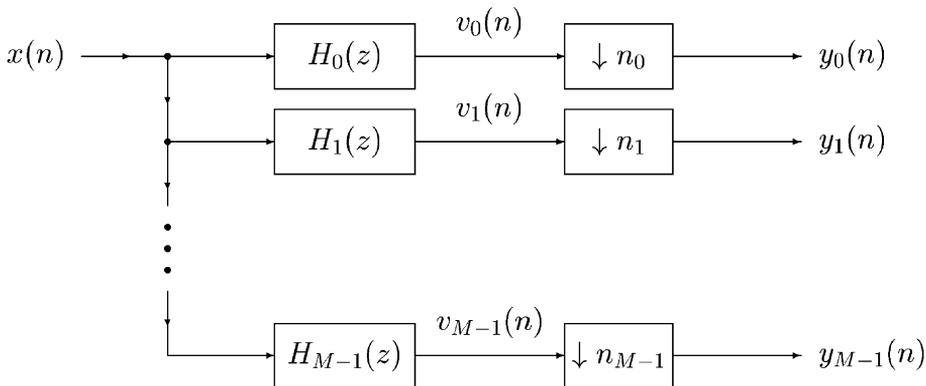$$[|H_i(e^{j\omega})|^2]_{\downarrow n_i} = 1 \quad \forall i \tag{17}$$

Fig. 11. The M-channel nonuniform analysis bank.

and that the set of analysis filters satisfies a generalized version of the power complementary property [17], which is that,

$$\sum_{i=0}^{M-1} \frac{|H_i(e^{j\omega})|^2}{n_i} = 1 \quad \forall \omega. \tag{18}$$

With these three properties, we will prove that the weighted geometric mean of the spectral flatnesses in the subbands is greater than or equal to the flatness in the fullband. This property was first observed by Rao and Pearlman [8], but only proven for a special case as will be discussed below. It will be shown in three steps. The first step involves proving a theorem regarding the subband variances. For brevity, we define $L \triangleq \mathrm{lcm}\{n_i\}$.

Theorem 1 (Geometric mean of the subband variances). *We have*

$$\prod_{i=0}^{M-1} (\sigma_{y_i}^2)^{1/n_i} \leqslant \sigma_x^2,$$

with equality if $S_{xx}(e^{j\omega})$ is of the form $S_{xx}(e^{j\omega}) = C(e^{jL\omega})$ for some $C(e^{j\omega}) \geqslant 0$.

Proof. From (3.36) and (3.40) of [17], it can easily be shown that we have

$$\sigma_x^2 = \sum_{i=0}^{M-1} \frac{1}{n_i} \sigma_{y_i}^2$$

by using the power complementary property of (18). Applying the weighted arithmetic–geometric mean inequality [10] (see the appendix), we obtain

$$\prod_{i=0}^{M-1} (\sigma_{y_i}^2)^{1/n_i} \leqslant \sum_{i=0}^{M-1} \frac{1}{n_i} \sigma_{y_i}^2,$$

which then proves the inequality. If $S_{xx}(e^{j\omega}) = C(e^{jL\omega})$, for some $C(e^{j\omega}) \geqslant 0$, note that we have, for any $i = 0, \ldots, M-1$ and $l = 0, \ldots, n_i - 1$,

$$S_{xx}(e^{j((\omega - 2\pi l)/n_i)}) = C(e^{jN_i(\omega - 2\pi l)}) = C(e^{jN_i\omega})$$

where $N_i \triangleq L/n_i$ is an integer for all i. Then, it can easily be shown that

$$S_{y_i y_i}(e^{j\omega}) = C(e^{jN_i\omega}),$$

using the Nyquist(n_i) property from [17]. From this, a straightforward calculation shows that,

$$\sigma_{y_i}^2 = \sigma_x^2$$

from which we obtain

$$\prod_{i=0}^{M-1} (\sigma_{y_i}^2)^{1/n_i} = (\sigma_x^2)^{\sum_{i=0}^{M-1} 1/n_i} = \sigma_x^2.$$

The last step here follows from the fact that the filter bank is maximally decimated (16). This completes the proof. $\square$

We now prove a result regarding the quantity ψ given in (15).

Theorem 2 (Arithmetic mean of the subband ψ's). *We have*

$$\sum_{i=0}^{M-1} \frac{1}{n_i} \psi_{y_i} \geqslant \psi_x$$

with equality iff $S_{xx}(e^{j\omega})$ is of the form $S_{xx}(e^{j\omega}) = C(e^{jL\omega})$ for some $C(e^{j\omega}) \geqslant 0$.

Proof. From the log-sum inequality [18] (see the appendix), if a_l and b_l are nonnegative numbers for $l \in \mathscr{I}$, where $\mathscr{I}$ is some index set, and the sequence $\{a_l\}$ is a probability density function (pdf) such that $\sum_{l \in \mathscr{I}} a_l = 1$, then we have

$$\ln\left(\sum_{l \in \mathscr{I}} b_l\right) \geqslant \sum_{l \in \mathscr{I}} a_l \ln \frac{b_l}{a_l}$$

with equality iff $b_l = Ka_l$ for all l and for some $K \geqslant 0$. Hence, for any pdf $\{a_{l,i}\}$ such that $\sum_{l \in \mathscr{I}_i} a_{l,i} = 1$ for all $i = 0, \ldots, M-1$, where $\mathscr{I}_i = \{0, \ldots, n_i - 1\}$, we have, as the psd of any random process is nonnegative,

$$\ln\left(\frac{1}{n_i}\sum_{l=0}^{n_i-1} S_{v_i v_i}(e^{j((\omega-2\pi l)/n_i)})\right) \geqslant \sum_{l=0}^{n_i-1} a_{l,i} \ln\left(\frac{(1/n_i)S_{v_i v_i}(e^{j((\omega-2\pi l)/n_i)})}{a_{l,i}}\right) \quad \forall \omega, i$$

with equality iff $(1/n_i)S_{v_i v_i}(e^{j((\omega-2\pi l)/n_i)}) = K_i a_{l,i}$ for all l, i where $K_i \geqslant 0$ for all i. Let us choose $a_{l,i}$ as $a_{l,i} = (1/n_i)|H_i(e^{j((\omega-2\pi l)/n_i)})|^2$ for all l, i. This choice is valid since by (17), we have

$$\frac{1}{n_i}\sum_{l=0}^{n_i-1} |H_i(e^{j((\omega-2\pi l)/n_i)})|^2 = 1 \quad \forall i$$

and so indeed $\{a_{l,i}\}$ is a pdf for all i. With this choice, we have, for all ω, i.

$$\ln\left(\frac{1}{n_i}\sum_{l=0}^{n_i-1} S_{v_i v_i}(e^{j((\omega-2\pi l)/n_i)})\right)$$

$$\geqslant \sum_{l=0}^{n_i-1} \frac{1}{n_i}|H_i(e^{j((\omega-2\pi l)/n_i)})|^2 \ln\left(\frac{(1/n_i)S_{v_i v_i}(e^{j((\omega-2\pi l)/n_i)})}{(1/n_i)|H_i(e^{j((\omega-2\pi l)/n_i)})|^2}\right)$$

$$= \frac{1}{n_i}\sum_{l=0}^{n_i-1} |H_i(e^{j((\omega-2\pi l)/n_i)})|^2 \ln\left(S_{xx}(e^{j((\omega-2\pi l)/n_i)})\right) \tag{19}$$

with equality iff $S_{xx}(e^{j((\omega-2\pi l)/n_i)}) = K_i$ for all ω, l, i. This condition for equality is equivalent to saying that $S_{xx}(e^{j\omega})$ is periodic with period $2\pi/L$. As the above is true for all ω, we thus have the following:

$$
\begin{aligned}
\psi_{y_i} &= \frac{1}{2\pi} \int_{-\pi}^{\pi} \ln\left(\frac{1}{n_i} \sum_{l=0}^{n_i-1} S_{v_i v_i}(e^{j((\omega-2\pi l)/n_i)})\right) d\omega \\
&\geqslant \frac{1}{2\pi n_i} \sum_{l=0}^{n_i-1} \int_{-\pi}^{\pi} |H_i(e^{j((\omega-2\pi l)/n_i)})|^2 \ln\left(S_{xx}(e^{j((\omega-2\pi l)/n_i)})\right) d\omega \\
&= \frac{1}{2\pi} \sum_{l=0}^{n_i-1} \int_{-\pi-2\pi l/n_i}^{\pi-2\pi l/n_i} |H_i(e^{j\lambda})|^2 \ln\left(S_{xx}(e^{j\lambda})\right) d\lambda \\
&= \frac{1}{2\pi} \int_{-\pi}^{\pi} |H_i(e^{j\omega})|^2 \ln(S_{xx}(e^{j\omega})) d\omega
\end{aligned}
\tag{20}
$$

It should be noted that this is true for all i with equality iff $S_{xx}(e^{j\omega})$ is of the form $S_{xx}(e^{j\omega}) = C(e^{jL\omega})$ for some $C(e^{j\omega}) \geqslant 0$. As (20) is true for all i, we have,

$$
\begin{aligned}
\sum_{i=0}^{M-1} \frac{1}{n_i} \psi_{y_i} &\geqslant \frac{1}{2\pi} \int_{-\pi}^{\pi} \left(\sum_{i=0}^{M-1} \frac{|H_i(e^{j\omega})|^2}{n_i}\right) \ln(S_{xx}(e^{j\omega})) d\omega \\
&= \frac{1}{2\pi} \int_{-\pi}^{\pi} \ln\left(S_{xx}(e^{j\omega})\right) d\omega = \psi_x.
\end{aligned}
\tag{21}
$$

Here, (21) follows from the generalized power complementary property (18). As we have equality iff $S_{xx}(e^{j\omega})$ is of the form $S_{xx}(e^{j\omega}) = C(e^{jL\omega})$, this completes the proof of Theorem 2. $\square$

From Theorem 2, we have the following important corollary if the input process $x(n)$ is Gaussian. This is important from the point of view of information theory. It is a generalization of a result given originally by Rao and Pearlman [8], in which only ideal analysis filters were considered and the authors eventually restricted the n_i's to be identical for all i.

Corollary 1 (Differential entropy rate). *If the input $x(n)$ to the nonuniform filter bank in Fig. 11 is a Gaussian WSS process and h_x and h_{y_i} denote, respectively, the differential entropy rates of $x(n)$ and the ith subband process $y_i(n)$, then we have*

$$
\sum_{i=0}^{M-1} \frac{1}{n_i} h_{y_i} \geqslant h_x
$$

with equality iff $S_{xx}(e^{j\omega})$ is of the form $S_{xx}(e^{j\omega}) = C(e^{jL\omega})$ for some $C(e^{j\omega}) \geqslant 0$.

Proof. If $x(n)$ is Gaussian, then its differential entropy rate is given by [18] to be

$$
h_x = \frac{1}{2} \ln(2\pi e) + \frac{1}{4\pi} \int_{-\pi}^{\pi} \ln(S_{xx}(e^{j\omega})) d\omega = \frac{1}{2} \ln(2\pi e) + \frac{1}{2} \psi_x.
$$

As $x(n)$ is assumed Gaussian, it follows that the signals $v_i(n)$ are also Gaussian, since the analysis filters $\{H_i(z)\}$ are linear. Furthermore, as $v_i(n)$ is Gaussian for all i, it follows that $y_i(n)$ is Gaussian for all i as well, since decimators are also linear systems. Hence, the differential entropy rate of $y_i(n)$ is given by

$$h_{y_i} = \tfrac{1}{2}\ln(2\pi e) + \tfrac{1}{2}\psi_{y_i}.$$

So, using Theorem 2 and the fact that the filter bank is maximally decimated (16), we immediately obtain

$$\sum_{i=0}^{M-1} \frac{1}{n_i} h_{y_i} \geqslant \frac{1}{2}\ln(2\pi e) + \frac{1}{2}\psi_x = h_x$$

with equality iff $S_{xx}(e^{j\omega}) = C(e^{jL\omega})$. This completes the proof.   □

We now conclude this section with the main result regarding the geometric mean of the flatness measures of the subband signals.

Theorem 3 (Geometric mean of the subband flatness measures). *Let the input to the analysis filter bank of Fig. 11 be a WSS random process $x(n)$ with spectral flatness measure γ_x^2. If the filter bank is such that (16)–(18) hold, then we have*

$$\gamma_y^2 \triangleq \prod_{i=0}^{M-1} (\gamma_{y_i}^2)^{1/n_i} \geqslant \gamma_x^2$$

with equality if $S_{xx}(e^{j\omega})$ is of the form $S_{xx}(e^{j\omega}) = C(e^{jL\omega})$ for some $C(e^{j\omega}) \geqslant 0$ where $L = lcm\{n_i\}$.

Proof. We have the following.

$$\gamma_y^2 = \frac{\exp(\sum_{i=0}^{M-1} (1/n_i)\psi_{y_i})}{\prod_{i=0}^{M-1} (\sigma_{y_i}^2)^{1/n_i}} \geqslant \frac{\exp(\sum_{i=0}^{M-1} (1/n_i)\psi_{y_i})}{\sigma_x^2} \geqslant \frac{e^{\psi_x}}{\sigma_x^2} = \gamma_x^2. \tag{22}$$

Here, (22) results from first using Theorem 1 and then using Theorem 2 and the fact that the exponential function is a monotonic increasing function. As a sufficient condition for equality in (22) is that $S_{xx}(e^{j\omega}) = C(e^{jL\omega})$ for some $C(e^{j\omega}) \geqslant 0$, this completes the proof.   □

This theorem is a generalization and a correction of a result given by Rao and Pearlman [8]. In that paper, only ideal analysis filters were considered and their expression for the analysis filter responses given in Eq. (1) was erroneous. At this point, we now proceed to present various examples of Theorem 3.

7. Examples of noise flattening in the subbands

In all of the following examples, we will assume that the noise process $\eta(n)$ is a real ARMA(18,17) process with psd shown in Fig. 12. The spectral flatness measure for this particular process was calculated numerically to be $\gamma_\eta^2 = 0.7680$.

Example 1. *The 2×2 Karhunen–Loève transform.* Consider the 2×2 paraunitary filter bank shown in Fig. 13. Here, **T** is the 2×2 KLT which is simply a scaled version of the 2×2 DFT matrix as is seen below.

$$\mathbf{T} = \frac{1}{\sqrt{2}} \begin{bmatrix} 1 & 1 \\ 1 & -1 \end{bmatrix} \Rightarrow H_0(z) = \frac{1}{\sqrt{2}}(1 + z^{-1}), \quad H_1(z) = \frac{1}{\sqrt{2}}(1 - z^{-1})$$

The flatness measures $\gamma_{\eta_0}^2$ and $\gamma_{\eta_1}^2$ are listed in Table 4. There, the geometric mean of the flatness measures in the subbands is denoted as $\gamma_{\eta,gm}^2$. Notice here that $\gamma_{\eta_0}^2$ is less than γ_η^2, but that $\gamma_{\eta_1}^2$ is greater than γ_η^2. More importantly, note that $\gamma_{\eta,gm}^2$ is greater than γ_η^2, in accordance with Theorem 3. As the flatness actually decreased in the 0th subband as compared with that of the fullband, it follows that the noise in that subband is less "white" than the input noise. Though this may appear discouraging at this point, we will soon see that with the analysis filters used in the examples in Section 4, the flatness seen in each subband will be strictly larger than that of the fullband.
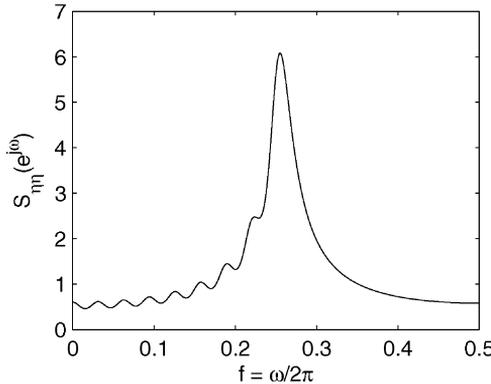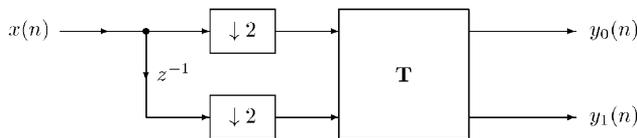

Fig. 12. Input noise power spectrum.

Fig. 13. The 2×2 Karhunen–Loève transform.

Table 4
Table of spectral flatness measures for Examples 1–4 ($\gamma_\eta^2 = 0.7680$)

Flatness	Example			
	2×2 KLT	Kaiser CMFB	DCT IV	Nonuniform FB
$\gamma_{\eta_0}^2$	0.7658	0.9935	0.9952	0.7678
$\gamma_{\eta_1}^2$	0.7801	0.9908	0.9904	0.8204
$\gamma_{\eta_2}^2$		0.9799	0.9951	0.9921
$\gamma_{\eta_3}^2$		0.9039	0.9021	0.9949
$\gamma_{\eta_4}^2$		0.9122	0.9241	
$\gamma_{\eta_5}^2$		0.9789	0.9995	
$\gamma_{\eta_6}^2$		0.9949	0.9948	
$\gamma_{\eta_7}^2$		0.9982	0.9993	
$\gamma_{\eta,gm}^2$	0.7729	0.9683	0.9744	0.8326

Example 2. *Kaiser–Window designed prototype cosine modulated filter bank*. If the noise process $\eta(n)$ from above is input to the filter bank described in Example 1 of Section 4, we obtain the subband flatness measures shown in Table 4. We can see that the flatness of each subband increased quite substantially over that of the fullband. Note that $\gamma_{\eta,gm}^2$ is greater than γ_η^2 in accordance with Theorem 3, even though properties (17) and (18) are only approximately satisfied for this choice of analysis bank.

Example 3. *DCT IV filter bank*. Applying $\eta(n)$ from above to the filter bank described in Example 2 of Section 4, we obtain the subband flatness measures shown in Table 4. As with the Kaiser–window designed filter bank, the flatness of each subband is significantly larger than that of the fullband. Note that $\gamma_{\eta,gm}^2$ is greater than γ_η^2, further verifying Theorem 3.

Example 4. *Binary tree-structured filter bank*. Thus far, we have only shown examples of Theorem 3 for uniform filter banks, even though this theorem also holds true for nonuniform filter banks as well. Consider the 3-level binary tree-structured filter bank shown in Fig. 14. The analysis filters are given as

$$H_0(z) = H(z),$$

$$H_1(z) = G(z)H(z^2),$$

$$H_2(z) = G(z)G(z^2)H(z^4),$$

$$H_3(z) = G(z)G(z^2)G(z^4).$$

Here $G(z)$ and $H(z)$ are, respectively, the lowpass and highpass filters associated with the Daubechies 16 wavelet [19]. The magnitude responses of the analysis filters are plotted in Fig. 15. It should be noted that with this choice of analysis filters,
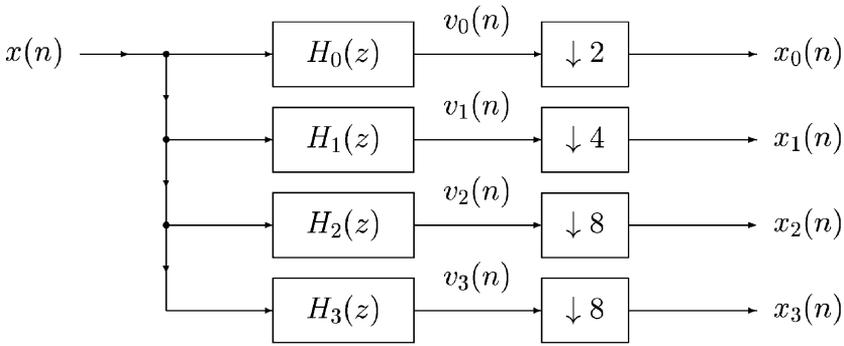
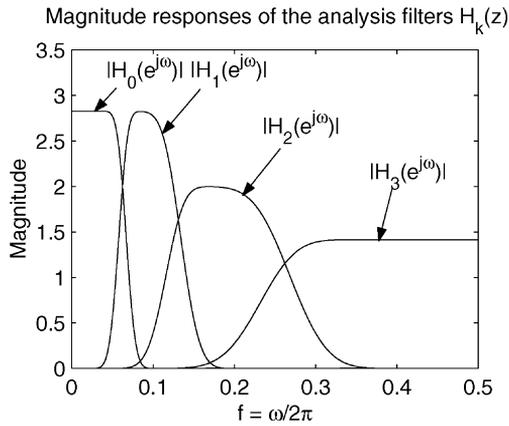Fig. 14. Nonuniform binary tree-structured analysis bank.

Fig. 15. Magnitude responses of the analysis filters for Example 4.

properties (16)–(18) are satisfied as desired. By applying the noise process $\eta(n)$ from above, we obtain the subband spectral flatness measures shown in Table 4. From this, we can see that the flatness actually decreased in the 0th subband but was significantly larger than the fullband flatness in the other subbands. As expected, $\gamma^2_{\eta,gm}$ is greater than γ^2_x, in accordance with Theorem 3.

Example of frequency estimation in the subbands with colored noise. Let the input to the Kaiser–window based filter bank of Example 1 in Section 4 be the following signal.

$$x(n) = \sqrt{2}\cos(\omega_1 n + \phi_1) + \sqrt{2}\cos(\omega_2 n + \phi_2) + \eta(n),$$
$$\omega_1 = 0.555\pi, \quad \omega_2 = 0.57\pi,$$

where $\eta(n)$ has the psd shown in Fig. 12. Note that both frequencies fall in the 4th subband. If the noise input statistics are not known a priori and we construct the
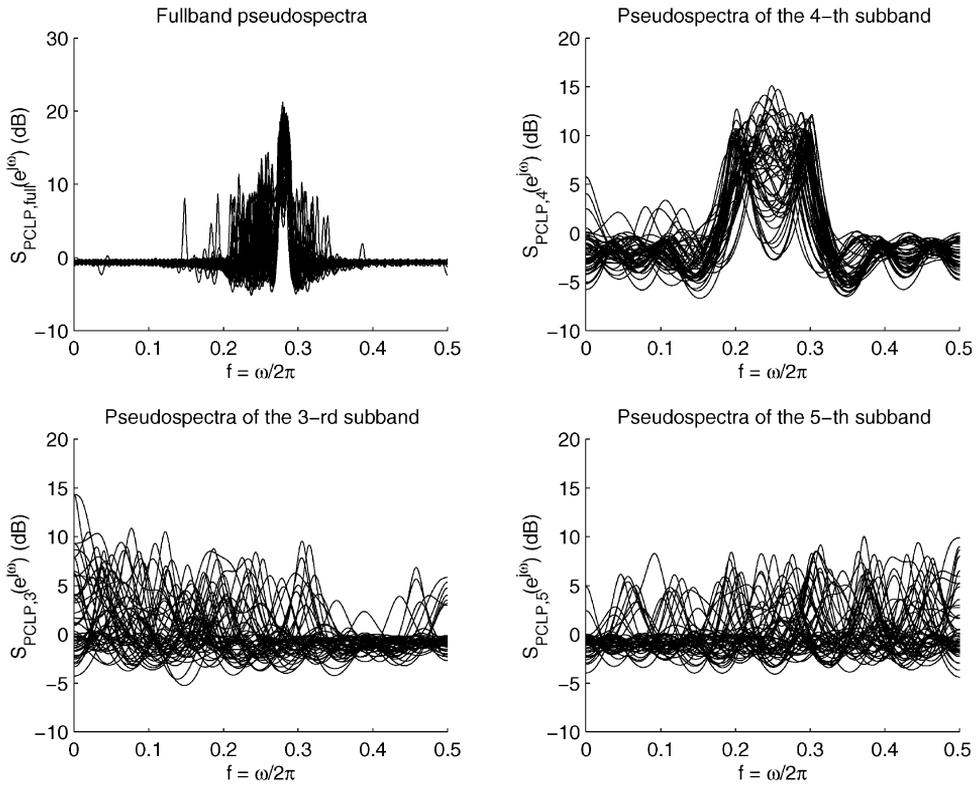
Fig. 16. Pseudospectra obtained for the case of colored noise (Kaiser CMFB).

Table 5
Comparison of fullband and subband methods for the case of colored input noise

Method	$\bar{\omega}_1(\omega_1 = 0.555\pi)$	$\bar{\omega}_2(\omega_2 = 0.57\pi)$	$\sigma\bar{\omega}_1$	$\sigma\bar{\omega}_2$
Fullband	0.5207π	0.5747π	0.01501	0.00928
Subband	0.5535π	0.5708π	0.000092	0.000098

pseudospectra just as before for the case of white noise, then we get the pseudospectra shown in Fig. 16. As with the examples of Section 4, pseudospectra for 50 independent observations of $x(n)$ were plotted. From the plots, we can see that there are two peaks in both the fullband pseudospectra, as well as in the 4th subband. The mean and standard deviation of the estimates of ω_1 and ω_2 carried out in both the fullband and in the subbands is shown in Table 5. From this, we can see that while the fullband pseudospectra consists of two dominant peaks, the location of these peaks is farther away from the true values than those seen in the pseudospectra of the 4th subband. The flatter noise seen in the subbands perturbed the peaks in their pseudospectra less than the heavily colored input noise perturbed the peaks of the fullband pseudospectra. This example justifies the notion that there

indeed are cases where we may assume that the noise in the subbands is practically white, even though this may not be the case in the fullband.

8. Concluding remarks

We have shown various ways in which frequency estimation in the subbands of a filter bank can perform better than conventional methods in the fullband, both theoretically and with numerous examples. It should be noted, however, that there are still a number of open problems that remain regarding this subject. For example, the statistical bias and variance of the frequency estimates have not been calculated and it is not known quantitatively how close the variance comes to the Cramér–Rao bound for frequency estimation. Such analysis will most likely shed more light on the precise tradeoff between the analysis filters and decimation ratios used and the number of observation samples available at each subband.

Another open problem stems from the result proven in Theorem 3. Given that the geometric mean of the flatness measures of the subband signals is always greater than or equal to that of the fullband input signal, provided that (16)–(18) are satisfied, the question then arises as to how to choose the analysis filters such that this geometric mean in maximized. This problem is probably more of theoretical than practical importance. The reason for this is because the optimal choice of analysis filters will most likely depend on the input statistics, which we have assumed here are not known a priori.

Appendix A. Important inequalities

A.1. Jensen's inequality

If $f(\mathbf{x})$ is a convex function for $\mathbf{x} \in \mathscr{D}$, where $\mathscr{D}$ is a convex set, then we have [20],

$$f\left(\sum_{i \in \mathscr{I}} \alpha_i \mathbf{x}_i\right) \leqslant \sum_{i \in \mathscr{I}} \alpha_i f(\mathbf{x}_i) \quad \text{where } \alpha_i \geqslant 0, \ \sum_{i \in \mathscr{I}} \alpha_i = 1 \tag{A.1}$$

Here, $\mathscr{I}$ is an index set and $\mathbf{x}_i \in \mathscr{D}$ for all i. Moreover, equality holds in (A.1) iff either the set of α_is is degenerate in the sense that $\alpha_i = 1$ for a particular i and is zero for the rest, or if $\mathbf{x}_k = \mathbf{x}_l$ for all k, l. Examples of convex functions are $f(x) = x^2$ and $f(x) = e^x$.

A.2. Weighted arithmetic–geometric mean inequality

Applying Jensen's inequality to the strictly convex function $f(x) = -\ln x$ over the interval $(0, \infty)$ yields the following important inequality [10].

$$\sum_{i \in \mathscr{I}} \alpha_i x_i \geqslant \prod_{i \in \mathscr{I}} x_i^{\alpha_i}$$

where the α_is are as in (A.1) and $x_i \geqslant 0$ for all i. The conditions for equality are the same as those for Jensen's inequality.

A.3. Log-sum inequality

From [18], we have the following inequality, which results from applying Jensen's inequality to the strictly convex function $f(x) = x \ln x$ over the interval $(0, \infty)$.

$$\sum_{i \in \mathscr{I}} a_i \ln \frac{a_i}{b_i} \geqslant \left(\sum_{i \in \mathscr{I}} a_i \right) \ln \frac{\sum_{i \in \mathscr{I}} a_i}{\sum_{i \in \mathscr{I}} b_i}$$

Here $a_i, b_i \geqslant 0$ for all i and we have equality iff $b_i = K a_i$ for all i and for some $K \geqslant 0$. If the sequence $\{a_i\}$ is a pdf in the sense that $\sum_{i \in \mathscr{I}} a_i = 1$, we obtain, $\ln(\sum_{i \in \mathscr{I}} b_i) \geqslant \sum_{i \in \mathscr{I}} a_i \ln (b_i/a_i)$.

References

[1] C.W. Therrien, Discrete Random Signals and Statistical Signal Processing, Prentice-Hall, Englewood Cliffs, NJ, 1992.
[2] S.M. Kay, Modern Spectral Estimation, Prentice-Hall, Englewood Cliffs, NJ, 1988.
[3] M.H. Hayes, Statistical Digital Signal Processing and Modeling, Wiley, New York, NY, 1996.
[4] D.H. Johnson, D.E. Dudgeon, Array Signal Processing, Prentice-Hall, Englewood Cliffs, NJ, 1993.
[5] S.U. Pillai, Array Signal Processing, Springer, New York, NY, 1989.
[6] S. Haykin (Ed.), Array Signal Processing, Prentice-Hall, Englewood Cliffs, NJ, 1985.
[7] A. Samant, S. Shearman, High-resolution frequency analysis with a small data record, IEEE Spectrum 36 (9) (1999) 82–86.
[8] S. Rao, W.A. Pearlman, Analysis of linear prediction, coding, and spectral estimation from subbands, IEEE Trans. Inform. Theory 42 (4) (1996) 1160–1178.
[9] P.P. Vaidyanathan, Multirate Systems and Filter Banks, Prentice-Hall, Englewood Cliffs, NJ, 1993.
[10] R.A. Horn, C.R. Johnson, Matrix Analysis, Cambridge Univ. Press, Cambridge, UK, 1985.
[11] V.F. Pisarenko, The retrieval of harmonics from a covariance function, Geophys. J. Roy. Astron. Soc. 33 (1973) 347–366.
[12] R. Schmidt, Multiple emitter location and signal parameter estimation, In Proc. RADC Spectrum Estimation Workshop 1979, pp. 243–258.
[13] D.W. Tufts, R. Kumaresan, Singular value decomposition and improved frequency estimation using linear prediction, IEEE Trans. Acoust. Speech, Signal Process. ASSP-30 (1982) 671–675.
[14] Y.P. Lin, P.P. Vaidyanathan, A Kaiser–Window approach for the design of prototype filters of cosine modulated filterbanks, IEEE Signal Process. Lett. 5 (6) (1998) 132–134.
[15] P. Yip, K.R. Rao, Discrete Cosine Transform: Algorithms, Advantages, Applications, Springer, New York, NY, 1997.
[16] N.S. Jayant, P. Noll, Digital Coding of Waveforms, Prentice-Hall, Englewood Cliffs, NJ, 1984.
[17] P.P. Vaidyanathan, Orthonormal and biorthonormal filter banks as convolvers, and convolutional coding gain, IEEE Trans. Signal Process. 41 (6) (1993) 2110–2130.
[18] T.M. Cover, J.A. Thomas, Elements of Information Theory, Wiley, New York, NY, 1991.
[19] G. Strang, T.Q. Nguyen, Wavelets and Filter Banks, Wellesly-Cambridge Press, Wellesly, MA, 1996.
[20] D.S. Mitrinović, Analytic Inequalities, Springer, New York, NY, 1970.